Multisensor approach to determine changes of wetland characteristics in semiarid environments (Central Spain)

Article *in* IEEE Transactions on Geoscience and Remote Sensing · December 2005

DOI: 10.1109/TGRS.2005.852082 · Source: IEEE Xplore

CITATIONS
91

READS
255

3 authors:

Thomas Schmid
Ciemat-Centro Investigaciones Energéticas, Medioambientales Y Tecnológicas
109 PUBLICATIONS **1,636** CITATIONS
SEE PROFILE

Magaly Koch
Boston University
193 PUBLICATIONS **1,875** CITATIONS
SEE PROFILE

Jose Gumuzzio
Boston University
20 PUBLICATIONS **291** CITATIONS
SEE PROFILE

Multisensor Approach to Determine Changes of Wetland Characteristics in Semiarid Environments (Central Spain)

Thomas Schmid, Magaly Koch, and Jose Gumuzzio

***Abstract*—Saline wetlands in the semiarid environment of Central Spain are fragile and highly dynamic ecosystems that are affected by degradation processes as a result of anthropological influences. An increase in agricultural production has led to the development of large-scale irrigation schemes with overexploitation of groundwater, and with consequent effects on the complex hydrology and associated land use. In this work, data from field, hyperspectral airborne, and multispectral satellite sensors are used in order to determine changes of wetland characteristics over time. The spectra of surface components (soil, vegetation, and salt crusts) were selected from the hyperspectral data and identified as endmembers using a site-specific spectral library. The spectral information contained in these endmembers was extrapolated to a temporal series of broadband multispectral imagery on which spectral unmixing analysis was performed in order to detect changes in the wetland over time. Results showed that the selected wetland components have undergone important changes in both their total area as well as their spatial distribution. These changes are mainly associated with the anthropogenic impact; however, natural influences due to seasonal fluctuations may coincide with the overall changes, although this in general is difficult to determine. Water regulation and agricultural practices directly influence the salinity of the soils and therefore the nature of the hygrophytic vegetation.**

***Index Terms*—Anthropogenic impact, change detection, multisensor, semiarid environments, spectral library, spectral unmixing, wetlands.**

I. Introduction

WETLAND areas are diverse and complex biophysical systems that frequently exhibit changes with respect to the spatial distribution, temporal duration, and spatial complexity of their components (soils, vegetation, water). In semiarid environments, wetlands are especially vulnerable to degradation processes, which influence the delicate balance between land and water processes. Climatic conditions of semiarid environments are the main influences that make these wetlands extremely fragile, which leads to naturally threatened ecosystems [1]–[3].

In the La Mancha Alta area of Central Spain, the semiarid wetlands are frequently saline and subsaline, and consist of numerous small wetlands (13–500 ha in area) peppering the landscape. These particular characteristics increase the difficulty of monitoring the wetland areas, which are especially important due to their role in maintaining and influencing environmental quality and biodiversity. These steppe wetlands are considered to be one of the most significant in Europe for migrating and wintering waterfowl [4], [5]. They are subject to natural (mainly seasonal) and, frequently, to human-induced changes. The factors that significantly alter the ecological functioning of these ecosystems include land use changes, where intensive agricultural cultivation replaces natural vegetation, overexploitation of ground water, desiccation and artificial drainage of wetlands, and the alteration and channeling of rivers. A combination of these factors is the major cause of wetland loss [2], [6] and the consequential alteration of the associated soils. The most recent inventory of the La Mancha Alta wetlands showed that 62.5% of wetland areas have disappeared or are in the process of disappearance and that, of the remaining wetlands, only 2.8% of the area is relatively well conserved [5].

Monitoring and controlling changes in the composition of the surface land cover (soil, vegetation, and water) in semiarid wetlands are essential tasks that often present practical difficulties. The first is to detect with sufficient precision, and often at different spatial scales, rapid changes in surface composition. The second difficulty is the problem of carrying out a multitemporal study on a long time scale to determine the direction and magnitude of these changes and thus assess the extent and degree of land degradation processes occurring in the wetlands.

In this respect, an important effort is taking place in the application of remote sensing techniques using data from hyperspectral and multispectral sensors in order to study these types of wetlands [7]–[10]. Related studies of importance within semiarid wetland areas are the mapping of soil properties, salinity, and vegetation [11]–[15]. The synergistic use of remotely sensed data from different sensors is an attractive alternative to characterize temporal and spatial changes of land surface features and conditions in wetland areas. Future monitoring studies will have to make retrospective use of today's multispectral data; therefore, a multisensor approach is seen as practical, and from an economic point of view, this could be a cost-saving approach.

The objective of this study is to determine land cover changes within semiarid wetland and surrounding upland areas using spectroscopic field, hyperspectral, and multispectral data representing different spatial and spectral scales. The period of interest is during the summer months when the wetlands are

Manuscript received November 1, 2004; revised March 23, 2005.

T. Schmid is with the Department of Environment, Research Centre for Energy, Environment and Technology (CIEMAT), E-28040 Madrid, Spain (e-mail: thomas.schmid@ciemat.es).

M. Koch is with the Center for Remote Sensing, Boston University, Boston, MA 02215 USA (e-mail: mkoch@bu.edu).

J. Gumuzzio is with the Department of Agricultural Chemistry, Geology, and Geochemistry, Autonomous University of Madrid, E-28049 Madrid, Spain (e-mail: jose.gumuzzio@uam.es).

Digital Object Identifier 10.1109/TGRS.2005.852082

least influenced by moisture, and there is an increase in salinity that affects the surface composition of the soil and vegetation distribution.

In this framework, spectral mixture analysis (SMA) [16]–[18] is used in order to determine landscape components and detect changes in their characteristics. SMA has several advantages over standard image classification methods. SMA is a physically based model that converts radiance/reflectance values to physical variables related to abundance of surface materials present within a pixel (i.e., classification is done in terms of endmembers and not in terms of statistical groupings). Second, it enables the detection and representation of components that occur at a spatial resolution that is smaller than the pixel size of moderate resolution instruments such as the Landsat Thematic Mapper (TM) and Enhanced Thematic Mapper (ETM+). An example is the distribution of sparse vegetation in arid and semiarid environments. Third, the data can provide quantitative results that can be used as inputs to models of the physical processes governing the distribution of surface materials within the image [19], [20].

Linear SMA is a well-established method to account for detail at the subpixel level and has been used extensively in a wide variety of studies of semiarid environments [21]–[23]. The endmember selection process is one of the most important aspects of SMA and has been the focus of much research [19], [24], [25]. Endmember identification and analysis are enhanced when high spatial and spectral resolution data are available, because such data can be used to represent subpixel variation in moderate resolution imagery. In this study, hyperspectral data were used to select representative endmembers. The endmembers are scene-specific, so once they are selected they can be used in spectral unmixing of images of the same area collected by different multispectral sensors [26]. Furthermore, the linear SMA model has been used in numerous change detection studies where the same set of endmembers has been applied to a temporal sequence of image data over a specific area [27]–[30]. Identifying spectral characteristics of wetland components using field spectrometry and relating the spectral curves of certain field samples with soil analytical and vegetation data provides an important support for characterizing these ecosystems in this work.

The value of remote sensing for the study of wetlands and the application of SMA for determining vegetation and soils is well documented. In this study, wetland components were identified using high spatial and spectral resolution data from a hyperspectral sensor and their spectral information was integrated as image-derived endmembers into the SMA. These endmembers are then used in the analysis of a temporal series of multispectral data with a significantly lower spectral and spatial resolution. This information is assessed quantitively in order to determine the capability of the SMA to extract abundance information for specific wetland cover types and detect changes with respect to the wetland areas. The contribution in this work is to demonstrate the complementary use of remotely sensed data together with the SMA technique to incorporate results derived from hyperspectral data into a temporal series of multispectral data.

Thus, the research reported in this paper has two main objectives. The first is to demonstrate that hyperspectral endmember spectra can be spectrally resampled to match the spectral resolution of a broadband sensor such as the Landsat TM and ETM+. The second objective is to demonstrate that endmembers selected from an image set with high spatial resolution can be successfully used to determine endmember proportions in lower resolution images. In effect, the higher spatial resolution data are providing subpixel level information for the analysis of the lower spatial resolution data. Hence, one would expect that endmembers selected from the higher spatial resolution image would better represent the true endmember spectrum than would an image endmember selected directly from the lower spatial resolution image.

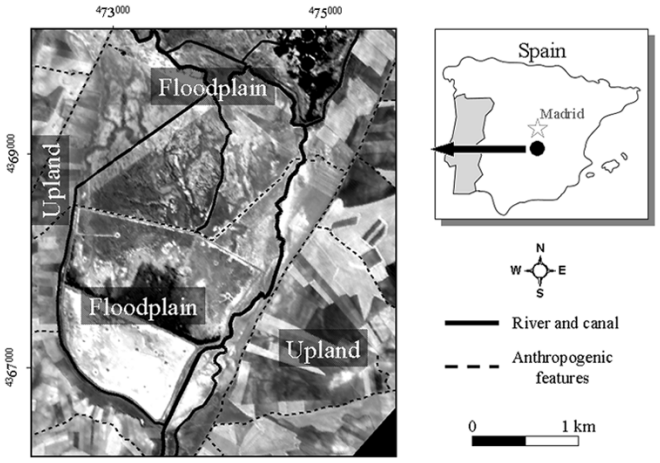

Fig. 1. Study area of the wetland in La Mancha Alta, Central Spain, showing the anthropogenic-affected floodplain and the surrounding upland.

II. Study Area

The study area is situated in Central Spain in the region of La Mancha Alta. The regional climate is classified as Mediterranean, with a continental character and semiarid nature. The landscape is dominated by an undulating topography at an average altitude of 650 m above sea level. The small river Gigüela meanders in a north–south direction forming a floodplain in the upper Guadiana River basin and is described as an anthropogenic affected floodplain, the Gigüela alluvial plain, [5] which covers an area of 500 ha (Fig. 1).

The wetlands are formed on Quaternary sediments that are generally rich in gypsum and calcium carbonates. Tertiary materials, mainly consisting of sandstone and limestone, surround the wetlands [31]. The soils of the wetlands are salt-affected with calcic, salic, and gypsic horizons and are classified as Sodic Calcisol, Gypsiric Cambisol, Gypsiric Regosol, and Typic Calcisol [32]. The soils of the upland areas around the floodplain are not salt-affected and are classified as Leptic Regosol and Calcaric Cambisol [32].

The natural vegetation of the wetland area is classified into hygrophytic (*Phragmites australis* and *Typha domingensis*) and halophytic species (*Salicornia europea*, *Suaeda vera*, *Puccinellia fasciculata*, *Limonium carpetanicum*, *Lygeum spartum*, and *Elymus curvifolius*) [33].

The floodplain area is strongly affected by anthropogenic activity and is divided into a number of private country estates. The main economic activities are hunting, livestock grazing, and crop cultivation. A series of anthropogenic influences have affected the flood plain area during the last few decades. In the early

1970s, modifications were carried out that included the construction of earth dykes and drainage ditches, and a permanent flooded area was created. During the second half of the 1980s, deepening and canalization of the Gigüela River was carried out. The aim was to divert water and reclaim wetlands further down river in the Tablas de Daimiel National Park. This action had important environmental impacts on the local hydrology and caused the destruction of riparian vegetation. Property owners are forbidden to divert river water to replenish their wetlands, and the consequence is their progressive desiccation. Further influences have been the conversion of the natural vegetation to agricultural uses and the plantation of trees over a wide area.

III. Materials and Method

A combination of data from field surveying, remote sensing, and ancillary data was used in this study. Spectroscopic data were obtained with an Analytic Spectral Devices FieldSpec Pro instrument during a field campaign conducted in June 2001. A site-specific spectral library was created [26], [34]. This library contains spectral information for the most representative wetland components (salt crusts, soil, and vegetation) together with soil sample analyses, vegetation classification, and ancillary topographic and meteorological data. Hyperspectral data were acquired by the Digital Airborne Imaging Spectrometer (DAIS 7915) on June 29, 2000. Multispectral Landsat TM and ETM+ data were obtained for June 17, 1987 and June 28, 2000, respectively. Data from the Advanced Spaceborne Thermal Emission and Reflection Radiometer (ASTER) was obtained for June 2, 2002.

Preprocessing of the DAIS 7915 data included radiometric, atmospheric, and geometric correction carried out by the German Aerospace Center (DLR) using the ATCOR4 and PARGE software [35], [36]. At the time of the overflight, a group of DLR experts operated a field spectrometer to obtain spectral calibration curves. These curves were used to calibrate the hyperspectral data to ground reflectance data. In the case of the multispectral Landsat and ASTER data, the radiometric and preliminary geometric corrections were carried out by the U.S. Geological Survey, National Center for Earth Resources Observation and Science (EROS), Sioux Falls, SD, and the Earth Remote Sensing Data Analysis Center (ERSDAC) in Japan, respectively. The Landsat data were acquired as a level 1G product, and the quantized pixel values were converted to exoatmospheric reflectance values using the calibration parameters for TM [37] and ETM+ [38]. The level 1B radiance data of ASTER was calibrated to at-satellite reflectance values [39]. All the multispectral images were recorded on cloud-free days. In order to remove any haze effects from the TM, ETM+, and ASTER images, a simple dark-object subtraction was applied [40]. This relative atmospheric correction was used to remove the variation within the scene and normalize the intensities between images collected on the different dates [41] using procedures available in the ENVI 4.0 software [42].

In part I of the methodological procedure (Fig. 2), key reference spectra representing the spectral properties of individual wetland components characterized by soil analysis and vegetation data were extracted from the spectral library. The characteristics of the spectral reflectance of the wetland components are well defined at the field scale. The spatial resolution of the field spectrometer is within the range of 10–20 cm, depending on the height of the sensor above the ground. As the spatial resolution of the DAIS hyperspectral sensor is 5 m, then a single DAIS resolution cell will consist of a mixture of different spectral components, each related to a particular land surface type. The same consideration can be made when using medium-resolution multispectral sensors, where the spectral signal is associated with a 30-m pixel. In this case, the signal will be composed of contributions from objects in a wider spatial area. Therefore, spectral field characteristics of several components were obtained along transects within selected test plots. These measurements were used as an aid in understanding the spectral heterogeneity within an area and matched with the spectral response obtained at a 5-m resolution such as the hyperspectral data.

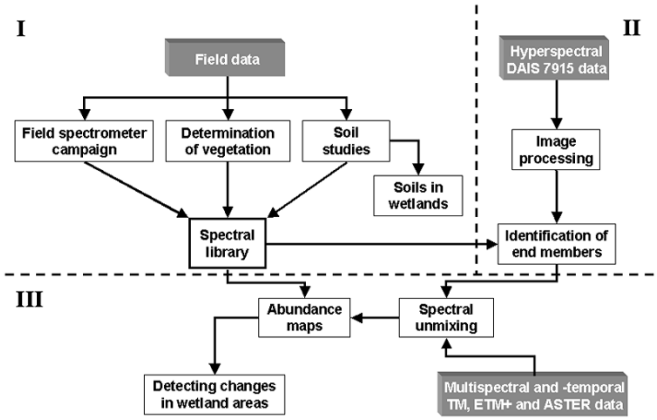

Fig. 2. Methodological procedure for carrying out a change detection analysis. Roman numerals I, II, and III indicate stages in the methodology used in this study.

In part II of the procedure (Fig. 2), the reflective bands of the DAIS 7915 sensor were used to determine surface features of wetland components. Image-derived endmembers were identified within the anthropogenic-affected flood plain area. Reference endmembers, derived from field measurements, undoubtedly represent more pure endmember spectra. However, image endmembers were obtained at the spatial scaling of the corresponding sensor and this determined the type of wetland component that would eventually be implemented. The DAIS 7915 imaging spectrometer contains 72 narrowband channels in the visible to the shortwave infrared (SWIR) spectrum (0.45–2.45 μm). The minimum noise fraction (MNF) procedure was used to transform the original data to a new dataset to reduce interband correlation and data redundancy [43], [44]. The inherent dimensionality of the data was taken to be equal to the number of eigenvalues whose magnitude exceeded 1.0 [43]. The selected MNF components were input to the pixel purity index (PPI) procedure [45], and using 50 000 iterations, the spectrally most pure pixels in the hyperspectral dataset were determined. The MNF and PPI results were then used as input to the n-dimensional visualizer [46] to determine spectral image-derived endmembers.

Knowledge of the spatial location of the individual image-derived endmembers allowed these endmembers to be identified

TABLE I
IMAGE-DERIVED ENDMEMBERS FOR THE SPECTRAL UNMIXING ANALYSIS

Endmember	Description	Feature characteristic
Hygrophytic vegetation	*Phragmites australis* and *Typha domingensis* enclosed by *Tamarix canariensis* (halophytic vegetation).	Thick vigorous vegetation and tree crowns found along the river and areas of water accumulation.
Wetland soil A	Desiccated exposed soil surface area with seasonal flooding.	Soil with abundant gypsum and 40% carbonate.
Wetland soil B	Cultivation practices of bare soil in fallow or sowed with crops.	Soil with very abundant gypsum and 20% carbonate with irregular surface due to ploughing.
Wet salt crust	Salt crust in depression areas along drainage ditches where soil surfaces are in exposed and moist conditions.	Composed of starkeyite, hexahydrite, gypsum and calcite.
Upland soil	Exposed cultivated soils in elevated areas surrounding the floodplain.	Very abundant phyllosilicates with an average of 10% carbonate content and 0.9% $Fe_2 0_3$.

in the hyperspectral dataset as well as in the field. Field verification is important. However, the endmembers representing the wetland components are highly variable in nature as their characteristics are influenced by the environmental conditions. Therefore, they were more difficult to verify as the conditions had changed by the time the data was ready for the processing and determination of the endmembers was carried out. Field surveys played an important role at the time of the data acquisition. The selected image-derived endmembers were compared to the key spectral curves contained in the spectral library using the spectral feature-fitting (SFF) algorithm [42], [47]. A pool of image-derived endmembers was acquired and identified via this matching procedure.

The change detection analysis, forming part III of the study methodology (Fig. 2), was performed using the temporal series of multispectral broadband Landsat TM, ETM+, and ASTER data from June 17, 1987, June 29, 2000, and June 2, 2002, respectively. An area of 3.75 km $\times$ 4 km (Fig. 1) was selected to represent the anthropogenic-affected floodplain and surrounding upland area. In order to be able to manage and relate the different image data, the multispectral data were spatially resampled and georeferenced to fit the 5-m spatial resolution of the hyperspectral data. The TM and ETM+ data were registered to the DAIS image using 17 ground control points (GCPs) and a first-order polynomial with a root mean square (RMS) error of 0.2066 and 0.2964 pixels, respectively. The ASTER data were registered using 20 GCPs and a first-order polynomial, which gave an RMS error of 0.2964 pixels. In each case, the RMS error refers to pixels with a dimension of 5 m. Spectral resampling of the hyperspectral image-derived endmembers was carried out to match the spectral characteristics of the multispectral data. The resampling method was carried out with the corresponding multispectral wavelengths (band centers) where a filter function [42] was applied using a Gaussian model with a full-width at half-maximum (FWHM) equal to the band spacings of the hyperspectral sensor.

A selection of image-derived endmembers corresponding to what were considered to be the most important characteristics of the wetlands and adjacent uplands were used for the spectral unmixing analysis. An unconstrained linear spectral unmixing model (LSUM) [48], [49] was applied, and according to the mathematical conditions of the model, a maximum of five endmembers was used [18], i.e., one less than the number of bands in the Landsat TM/ETM+ data, this being the sensor with the fewest number of bands. The same set of image-derived endmembers was used in the spectral unmixing analyses of the individual multispectral data, in order to establish the nature of any change in the spatial distribution and abundance of the individual wetland endmembers. A significance value of 5% was applied to the abundance images in order to identify change in the surface features represented by the individual endmembers. Change detection maps were produced by calculating the differences between the individual abundance maps for 1987 and 2000, and for 2000 and 2002.

IV. RESULTS AND DISCUSSION

The results focus on the implementation of high-resolution image-derived endmembers from the anthropogenic-affected floodplain and surrounding area using the LSUM and applying the multispectral data. Table I shows the five image endmembers selected for spectral unmixing and the final change detection analyses.

The spectral characteristics of the five endmembers were initially identified from the spectral curves obtained from the hyperspectral DAIS 7915 sensor [Fig. 3(a)].

The hygrophytic vegetation is vigorous, as confirmed by its spectral reflectance in the red/near-infrared region of the spectrum. Wetland soil A has a high reflectance in the visible and near-infrared range and is influenced by seasonal flooding with the formation of a smooth sediment surface composed of gypsum and carbonates. The spectral characteristics of wetland

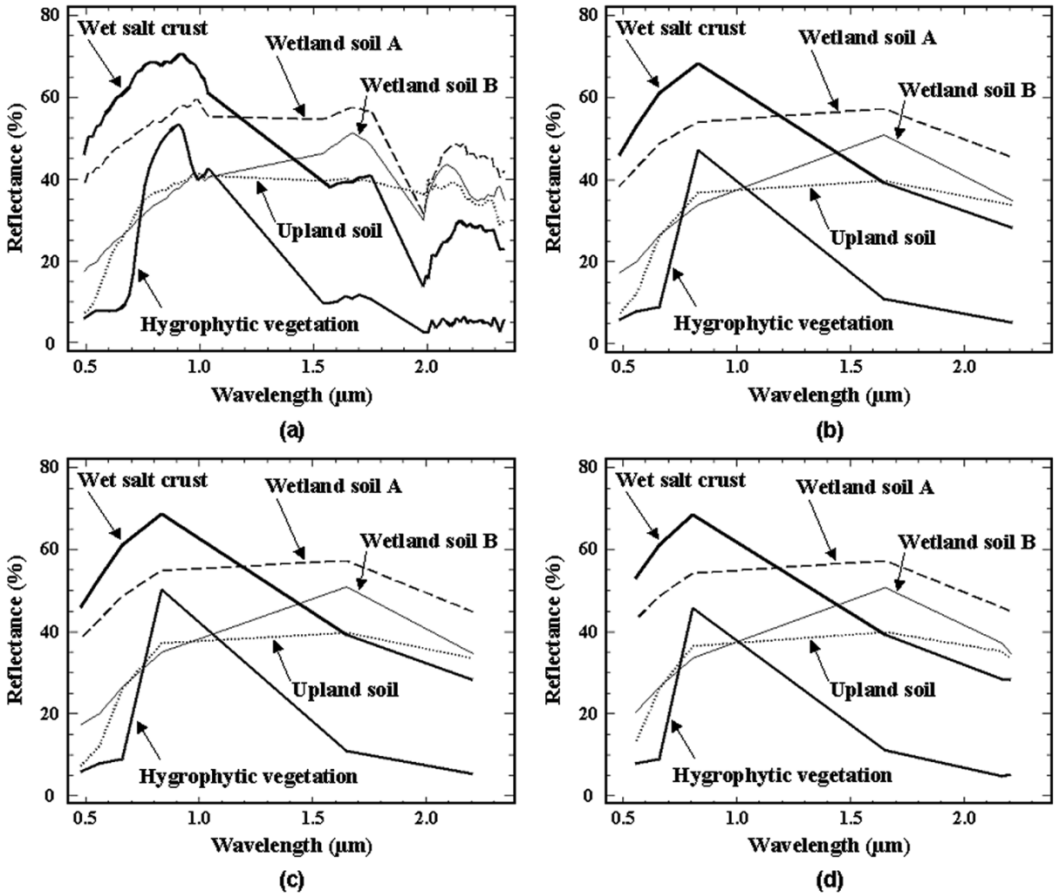

Fig. 3. Spectral transformation of the image-derived endmembers to the corresponding resolution of hyperspectral (a) DAIS 7915, and multispectral (b) Landsat TM, (c) Landsat ETM+, and (d) ASTER data.

soil B are again associated with gypsum and carbonates; however, the general reflectance is lower than that of wetland soil A. The difference is related to the physical characteristics, such as roughness of the soil surface as a result of ploughing. The wet salt crust shows high reflectance in the visible and VNIR wavebands (0.635 to 1.038 μm) and a decrease in the SWIR due to the moisture conditions. The spectral characteristics identified for the upland soil endmember are iron oxides and clay minerals at 0.87 and at 2.2 μm, respectively.

The individual image-derived endmembers were located in the hyperspectral data and their spatial coordinates were determined, to allow verification in the field. The field surveys and the spectral library [34] therefore played an important role at the time of data acquisition. Selected image-derived endmembers were verified with the key spectral curves contained in the spectral library and complementary information from the field was associated with the image-derived endmembers.

The transformation of these five endmembers from the hyperspectral to the multispectral resolution shows that important spectral characteristics are maintained at the corresponding wavelengths. The general form of the curves for the individual sensors is practically identical for Landsat TM [Fig. 3(b)] and ETM+ [Fig. 3(c)], with a slight variation being observed with the ASTER [Fig. 3(d)] endmembers. The reason for this slight variation is that the ASTER sensor does not have a band in the visible blue spectral region corresponding to the TM or ETM+ band 1, but has additional bands in the SWIR region. In this case, the change detection procedure has to accommodate the TM and ETM+ sensors with the smallest number of spectral bands. Therefore, the six ASTER bands were selected according to the wavelength of the band centers and the spectral range of the Landsat bands. Keeping the number of bands equal between the different multispectral sensors facilitates the comparison between sensor's performances.

The results of the spectral unmixing are in the form of abundance values or proportions that should lie, in theory, in the range 0–1. When the unconstrained model is used, proportions may lie outside this range due to one or more of the following reasons: 1) the linear mixture model does not adequately fit the data; 2) the endmembers are badly chosen and do not represent the extremes of the distribution of reflectance values for that endmember; 3) the number of endmembers is not sufficient to describe the dataset [18]. Table II lists the statistical properties of each endmember for the three dates (1987, 2000, and 2002).

The distributions of the abundance values for the individual endmembers were examined in terms of the three image dates. The minimum, maximum, mean, and standard deviation describe the distribution of the abundance values. The under- and overshoots together with the overall RMS value reflect the fit of the model. An example is the endmember representing the hygrophytic vegetation, which has an abundance range in the ETM+ 2000 image of -0.20 to 1.04. The mean value of 0.18

TABLE II
DESCRIPTIVE STATISTICS OF THE ENDMEMBERS

	Hygrophytic vegetation	Wetland soil A	Wetland soil B	Wet salt crust	Upland soil	RMS error
TM 1987						
Min	0.01	-0.55	-0.98	-0.74	-0.13	0.000
Max	0.52	1.32	0.86	0.63	1.12	0.015
Mean	0.13	0.51	-0.10	-0.27	0.42	0.007
Stdev	0.05	0.28	0.32	0.16	0.24	0.002
Percent < 0	0.00	4.00	60.18	94.60	0.64	0.00
Percent 0 - 1	100.00	93.05	39.82	5.40	99.21	100.00
Percent > 0	0.00	2.95	0.00	0.00	0.15	0.00
ETM+ 2000						
Min	-0.20	-1.73	-1.17	-0.81	-1.21	0.000
Max	1.04	2.18	3.20	1.18	0.93	0.030
Mean	0.18	0.31	0.34	-0.07	0.00	0.003
Stdev	0.15	0.39	0.37	0.21	0.29	0.002
Percent < 0	0.88	20.75	22.14	62.44	50.02	0.00
Percent 0 - 1	99.09	75.21	76.63	37.55	49.98	100.00
Percent > 0	0.03	4.04	1.23	0.01	0.00	0.00
ASTER 2002						
Min	-0.23	-0.94	-0.91	-1.18	-1.31	0.000
Max	0.99	2.61	1.09	0.66	0.80	0.019
Mean	0.17	0.72	-0.03	-0.35	0.07	0.003
Stdev	0.09	0.20	0.23	0.12	0.20	0.002
Percent < 0	1.34	0.20	55.91	98.49	43.62	0.00
Percent 0 - 1	98.66	93.78	44.09	1.51	56.38	100.00
Percent > 0	0.00	6.02	0.00	0.00	0.00	0.00

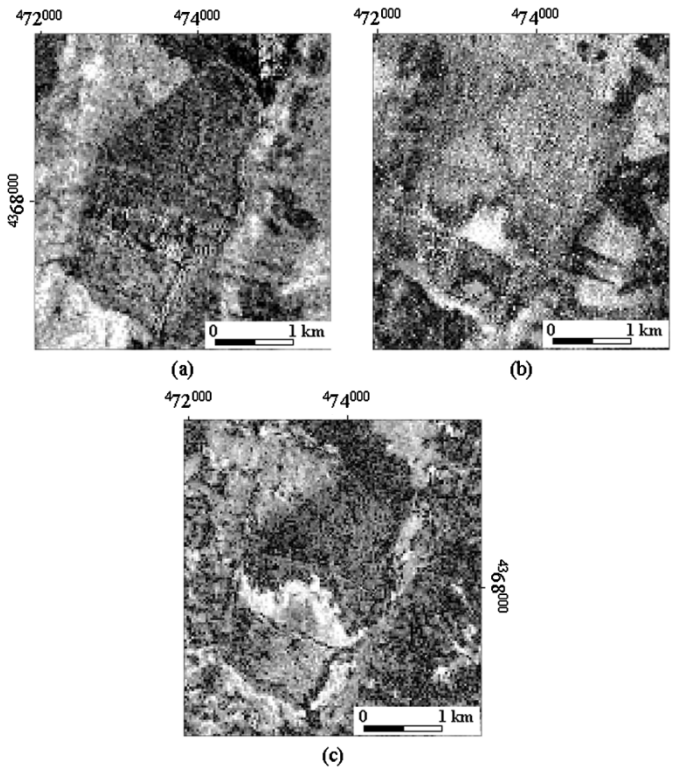

Fig. 4. RMS error image corresponding to the abundance of (a) TM on June 17, 1987, (b) ETM+ on June 28, 2000, and (c) ASTER on the June 2, 2002.

and a standard deviation of 0.15 indicate that the majority of the values lie within the 0–1 range. This is further shown by the percentage under- and overshoots, which are 0.88 and 0.03, respectively. It is important to note that, within the distribution of the abundances, at least one pixel has a value of 1, indicating a 100% pure endmember. This is achieved in this case, as the maximum value is 1.04. In comparison, the ASTER 2002 endmember shows a similar behavior. The maximum value is just under 1, but this result can be regarded as acceptable. In the case of the TM 1987, the endmember has a narrow range and low mean and standard deviation. The highest abundance value is just 0.52. This indicates the endmember has a maximum of 52% purity or representation in the pixel for the TM results and is less representative than in ETM+ and ASTER results. A similar analysis was followed for the remaining endmembers. The abundance distribution of wetland soil B for TM and ASTER data are within the expected range, whereas for the ETM+, an increase of undershoots is observed. Wetland soil B has abundance values, which indicate a considerable percentage of undershoots in the different image data. Therefore, this endmember is less representative of surface conditions than the first two endmembers. The abundance values for the salt crust endmember show negative mean values with low standard deviation for all the image dates. In the case of TM and ASTER, practically all the abundance values are undershoots. The ETM+ result is only slightly better. It seems as if the values have shifted into the negative scale. The results from this endmember are therefore to be treated with caution. The results for the upland endmember in the TM are well defined for the model, whereas the remaining two images ETM+ and ASTER do not fit the model so well.

The analysis of the RMS error value indicates the goodness of fit of the model. The higher the maximum RMS value the worse the model fit in terms of determining the distribution of the abundance values. The maximum RMS values attained in the TM, ETM+, and ASTER datasets were 0.015, 0.030, and 0.019, respectively. These values are low and lie within the range of acceptance [27], [50].

The RMS error images (Fig. 4) show that the LSUM has worked well for most of the area of the flood plain. The presence of coherent information in these RMS images shows that the set of endmembers is either too small or its members are badly chosen. Given that the endmembers were carefully selected using hyperspectral data verified with field spectra, one would conclude that the scene is too complex to be described by a set of five endmembers. In the TM, the upland area in the southern part of the image shows an area with bright pixels. This represents dry crop areas or the stubble and straw left on the ground after harvesting. The ETM+ and ASTER images show a significant area within the central part of the flood plain. This area has hygrophytic vegetation surrounded by a visible lamina of water, which is formed behind the earth dyke to create an artificial lagoon. Although vegetation seemed abundant when carrying out the field survey, water dominates the spectral characteristics with low reflectance values.

The RMS image is an important indicator of surface features that were not included in the LSUM. As mentioned earlier, only five endmembers can be used at any one time to carry out the LSUM. It is difficult to represent this kind of dynamic environment in terms of only five endmembers. Furthermore, an endmember that is present in one year is not necessarily present at another time. So the temporal aspect of the analysis complicates the selection of an ideal endmember combination.

The final combination of endmembers (Table I) was chosen after a number of tests of different image-derived endmembers from the pool of endmembers. Testing different combinations

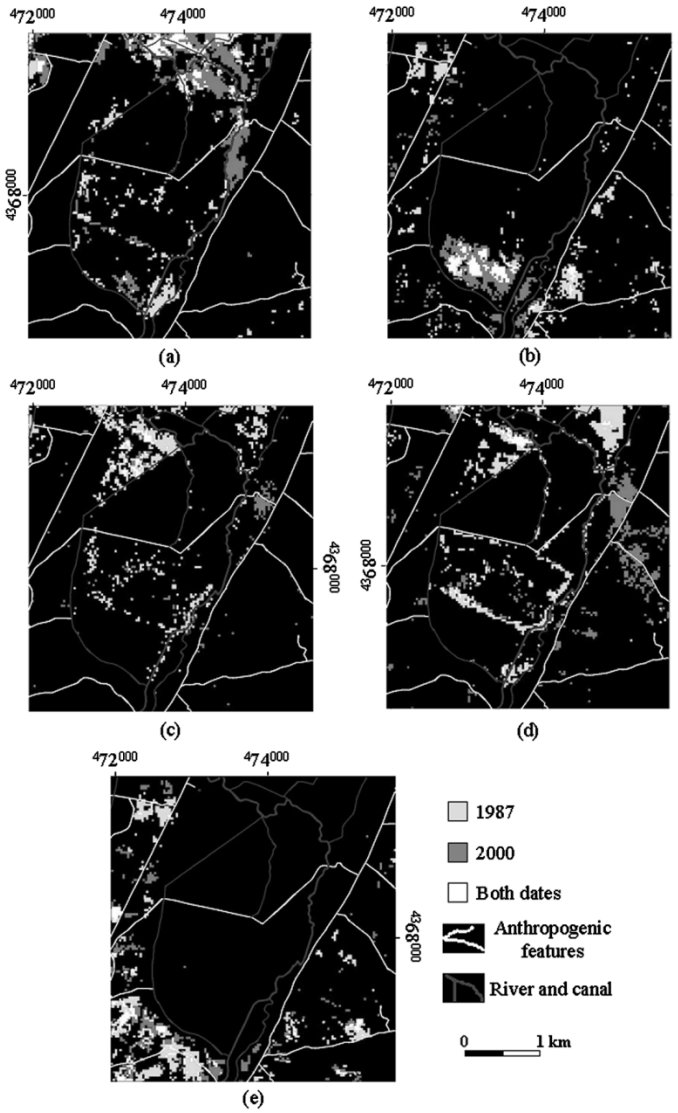

Fig. 5. Change detection analyses between TM (1987) and ETM+ (2000) for (a) hygrophytic vegetation, (b) wetland soil A, (c) wetland soil B, (d) wet salt crust, and (e) upland soil.

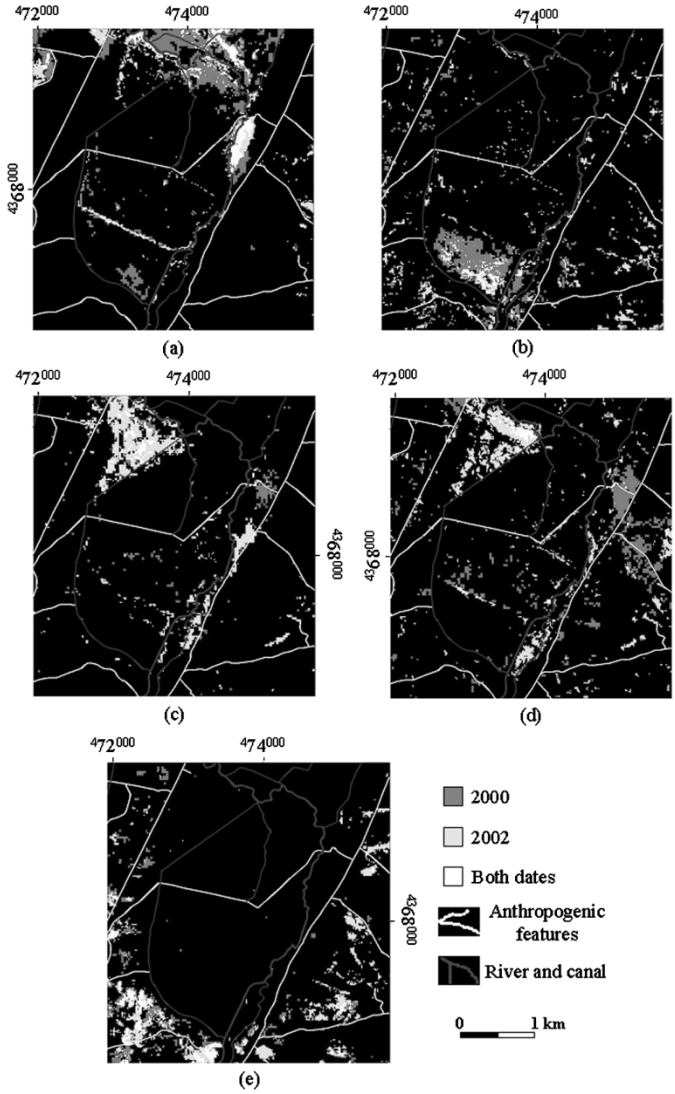

Fig. 6. Change detection analyses between ETM+ (2000) and ASTER (2002) for (a) hygrophytic vegetation, (b) wetland soil A, (c) wetland soil B, (d) wet salt crust, and (e) upland soil.

of endmembers is common practice, in order to evaluate the relation between the image-derived endmembers from hyperspectral data and the broadband imagery data, and to assess the model fit. A threshold value had to be determined in order to obtain the pixels with a high abundance value. In this case the threshold was set at 1.64 standard deviations, which means that the pixels will contain an abundance value that represents the corresponding endmember with no less than 95% purity. According to field verification, this threshold was considered the best value for comparison of the final abundances. In other words it represents the highest 5% of values within the abundance distribution. The same standard deviation was used with the remaining abundance images and the difference between the corresponding endmember abundances over the three dates was used to indicate the spatial change in that endmember.

Change detection was carried out using the TM and ETM+ data [Fig. 5(a)–(e)] and the ETM+ and ASTER data [Fig. 6(a)–(e)]. In the former case, change detection is applied to two multispectral (TM and ETM+) sensors with practically identical characteristics regarding the number and width of the reflective bands. In the latter case, the detection is between two sensors (ETM+ and ASTER) with different band characteristics. This type of temporal comparison will become more common as some remote sensing programmes (e.g., Landsat and SPOT) come to an end and data from new sensors becomes available.

The changes observed for the surface characteristics are closely related to the anthropogenic influences in this area. The dramatic change represented for the hygrophytic vegetation [Figs. 5(a) and 6(a)] is shown in the total surface area for 1987 (5.4%—81 ha), 2000 (7.8%—117 ha), and 2002 (4.5%—67.5 ha) and the corresponding spatial distribution. This is due to construction works on the river and coincides with a low annual rainfall during 1987 and the clearing of natural vegetation for cultivation practices carried out on the eastern flank of the wetland area for 2002.

Wetland soil A [Figs. 5(b) and 6(b)] represents a saline soil concentrated within a desiccated area in the southern part of

the floodplain area. The soil covers a total surface area of 4.1% (61.5 ha), 4.8% (72 ha), and 4.2% (63 ha) for 1987, 2000, and 2002, respectively. Although the total surface area is fairly constant, a spatial redistribution is observed between the image dates. The wetland soil is also identified in the upland area. An explanation is that elevated carbonate content in the soil from the desiccated area is similar to the content also present in upland soils where the spectral properties of carbonate influence the unmixing result.

Changes for the wetland soil B [Figs. 5(c) and 6(c)] is largely influenced by agricultural activities carried out along the east and west side of the flood plain. Following the yearly sequence of the former examples, the total surface area of 4.8% (72 ha), 2.0% (30 ha), and 5.5% (82.5 ha) indicates that higher values have more area as fallow and lower values means that a greater area of crops has been cultivated.

The distribution of the wet salt crust [Figs. 5(d) and 6(d)] is mainly found along drainage ditches and within depression areas. The total area occupied for the corresponding years of 1987, 2000, and 2002 are 5.8% (87 ha), 4.8% (72 ha), and 5.2% (78 ha), respectively. The spatial distribution in 1987 is again related to the construction works carried out on the river and the resulting drainage and exposure of soil surface areas within the floodplain where salt crusts formed. In 2000, an extensive wet salt crust area to the east of the flood plain area and extending into the upland area was identified. In this case, areas with ripe cereal crops were incorrectly identified as wet salt crust. As indicated above (Table II), the statistical distribution showed that the unmixing model for ETM+ was not able to determine the salt crust proportions with the required accuracy.

The distribution of the upland soils endmember [Figs. 5(e) and 6(e)] clearly discriminates the wetland and the upland areas and is correctly shown as being located in the elevated areas around the flood plain. In this case, the spatial distribution of nonvegetated upland soils changes yearly, depending on the management practices of the farmers and are as follows: 5% (75 ha), 4% (60 ha), and 5.1% (76.5 ha) for the respective years 1987, 2000, and 2002.

The general land surface conditions of the anthropogenically affected flood plain area show differences, especially for the period 1987–2000 (Fig. 5). This was expected, as human-induced changes have altered the general conditions by introducing major changes to the hydrology of the region. The management of this wetland is therefore important especially as this area is also used for both agricultural and recreational purposes. There are also the natural influences such as climate and the related dry period in the mid-1980s when a below-average precipitation in that period affected the entire region. However, this is difficult to interpret with these results, as this would require the processing and application of a temporal series consisting of yearly image data for a month such as June.

The change detection carried out with the selected combination of endmembers performed reasonably well. The LSUM was limited by the number of bands of the Landsat TM/ETM+ image (which has six reflective bands), which restricted the maximum number of endmembers to five. The choice of endmembers was clearly tilted in favor of wetland characteristics. Four of the five endmembers represented wetland surface components and only one upland component was considered. This limitation can cause other dominant characteristics to affect the final result of the unmixing model as was shown with ripe cereal crops in the upland area and with wet salt crust from the wetland area. However, areas of ripe crops can be readily identified in field surveys or from spectral analysis of the image. The important fact to note was that this salt crust was identified correctly in the area of study. Cereal crops could be used as an endmember and substituted for one of the other endmembers, but, this combination did not improve the overall result and interest of the distribution of the cereal crop was secondary.

The approach presented in this paper has shown that several advantages can be obtained from transferring hyperspectral endmembers to multispectral data. These include the following.

1) The ability to detect surface components in hyperspectral images that cannot be otherwise mapped with the same accuracy in lower resolution images. The 5-m resolution hyperspectral endmembers represent subpixel components of the medium-resolution TM, ETM+, and ASTER images. Such data cannot be derived directly from the medium spatial resolution data.
2) The ability to generalize endmember spectra from the hyperspectral data to the TM/ETM+ and ASTER data allows the use of sequences of multitemporal images and thus facilitate the identification and characterization of landscape change.
3) Results obtained from small test sites, which have been validated on the ground, can be extended to wider areas in semiarid environments.

The methodological approach described in this paper improves our ability to identify and delineate wetland components in semiarid environments, to select endmembers from the hyperspectral data, and to use these endmembers with multispectral data at different spatial and temporal scales. Field surveys played an important role to establish the corresponding characteristics found within these wetland types and to verify the results obtained at the different stages in the methodology.

V. Conclusion

A change detection based on linear spectral unmixing has been carried out successfully in a highly dynamic and anthropogenic-affected wetland area. However, the application of the LSUM is affected by the fact that the number of spectral bands in the multispectral images limits the number of endmembers that can be used simultaneously. Although summer was chosen as the time of year when the influence of moisture is a minimum, the complex diversity of these ecosystems need to be further investigated at the level of monitoring.

The method implemented in this work selects image-derived endmembers from high spatial and spectral resolution data enabling therefore certain surface features associated particularly to the wetland areas to be determined. The identification and application of selected endmembers is based on detailed data obtained at the field scale and related to the hyperspectral data. Resampling hyperspectral or high-resolution endmembers to the multispectral resolution does affect the level of detail of absorption features contained in wetland component spectra and

thus their reflective properties are less well defined as in the hyperspectral data. However, the general shape of the spectral reflectance curve is maintained and this information can therefore be applied to data archives such as the Landsat data enabling the detection of progressive changes over several decades.

A major contribution of this work is the capacity to use endmembers derived from hyperspectral information in the analysis of existing multispectral data from different sensors. In this case, the synergistic use of hyperspectral DAIS 7915 and multispectral Landsat and ASTER data is novel. The same approach can be used with other and future hyperspectral and multispectral sensors to enhance results and to follow up the monitoring. The methodology adopted here forms the basis to continue integrating data obtained from future sensors in order to delineate and monitor wetlands in semiarid environments. This leads to the appealing fact that this approach could be implemented to ecosystems throughout semiarid environments in different regions of the world. Results would almost certainly improve when applying this methodology to ecosystems that are less dynamic and complex.

ACKNOWLEDGMENT

The authors would like to thank and gratefully acknowledge the support of the following centers: the U.K. Natural Environment Research Council Equipment Pool for Field Spectroscopy, for the loan of the ASD FieldSpec Pro spectrometer; the German Aerospace Centre for providing the DAIS 7915 data, collected during the HySens Programme 2000–2003 (HS-2000ES2) and the corresponding preprocessing of the data; and the Japan Aerospace Exploration Agency (JAXA) for providing the ASTER image as part of the user proposal AP-0072. The authors would also like to give their sincerest thanks to P. M. Mather (Nottingham University) for his valuable comments and thorough revision of the manuscript.

REFERENCES

[1] S. Casado, M. Florin, S. Molla, and C. Montes, "Current status of Spanish wetlands. An ecological and conservation overview," in *Managing Mediterranean Wetlands and Their Birds for the Year 2000 and Beyond*, M. Finlayson, Ed. Slimbridge, U.K.: IWRB-ICBN, 1991, Special Publication no. 20, pp. 56–57.

[2] S. Casado and C. Montes, *Guía de Los Lagos y Humedales de España*. Madrid, Spain: J. M. Reyero, 1995, pp. 124–149.

[3] M. Florín, "Funciones y valores de los humedales manchegos," *Quercus*, vol. 163, pp. 10–18, Sep. 1999.

[4] A. del Moral, "Avifauna," in *Humedales de Ciudad Real*, 1st ed. Talavera de la Reina, Toledo, Spain: Esfagos S. L., 2000, pp. 112–123.

[5] G. Oliver and M. Florín, "The wetlands of La Mancha, Central Spain: Opportunities and problems concerning restoration," in *Bases Ecológicos Para la Restauración de Humedales en la Cuenca Mediterránea*, C. Montes, G. Oliver, F. Molines, and J. Cobos, Eds. Andalucía, Spain: Junta de Andalucía, Consejería de Medioambiente, 1995, pp. 197–216.

[6] S. Cirujano, "Flora y vegetación," in *Humedales de Ciudad Real*, 1st ed. Talavera de la Reina, Toledo, Spain: Esfagos S. L., 2000, pp. 124–131.

[7] Y. Nakayama, S. Tanaka, T. Sugimura, and K. Endo, "Analysis of hydrological changes in lakes of Asia arid zone by satellite data," *Proc. SPIE*, vol. 3222, pp. 201–210, 1997.

[8] M. Koch, T. F. Schmid, and J. Gumuzzio, "The study of anthropogenic affected wetlands in semi-arid environments applying airborne hyperspectral data," in *Teledetección, Medio Ambiente y Cambio Global*, J. Rosell Urrutia and J. Martínez-Casanovas, Eds. Lleida, Spain: Univ. Lleida Editorial Milenio, 2001, pp. 297–301.

[9] C. Castañeda, *El Agua de las Saladas de Monegros del Sur Estudiada con Datos de Campo y de Satélite*. Zaragoza, Spain: Consejo de Protección de la Naturaleza de Aragón, 2002, Serie Investigación, pp. 63–114.

[10] T. Schmid, M. Koch, S. Cirujano, and J. Gumuzzio, "Application of hyperspectral data to study saline wetland areas in semiarid environments," in *Teledetección y Desarrollo Regional*, R. Peréz Utrero and P. Martínez Cobo, Eds. Cáceres, Spain: Copegraf, 2003, pp. 451–456.

[11] B. Lacaze, V. Caselles, C. Coll, J. Hill, C. Hoff, S. de Jong, W. Mehl, J. F. W. Negendank, H. Riezebos, E. Rubio, S. Sommer, J. T. Filho, and E. Valor, "Integrated approaches to desertification mapping and monitoring in the Mediterranean basin, Final report of the DeMon-1 Project," Joint Res. Centre, Eur. Commiss., EUR 16448EN, 1996.

[12] E. Ben-Dor, K. Patkin, A. Banin, and A. Karnieli, "Mapping of several soil properties using DAIS-7915 hyperspectral scanner data—A case study over clayey soils in Israel," *Int. J. Remote Sens.*, vol. 23, no. 6, pp. 1043–1062, Mar. 2002.

[13] J. K. Crowley, "Mapping playa evaporite minerals with AVIRIS data: A first report from Death Valley, California," *Remote Sens. Environ.*, vol. 44, pp. 337–356, Jun. 1993.

[14] G. I. Metternicht and J. A. Zink, "Remote sensing of soil salinity: Potentials and constraints, Review article," *Remote Sens. Environ.*, vol. 85, pp. 1–20, Apr. 2003.

[15] G. S. Okin, D. A. Roberts, B. Murray, and W. J. Okin, "Practical limits on hyperspectral vegetation discrimination in arid and semiarid environments," *Remote Sens. Environ.*, vol. 77, pp. 212–225, Aug. 2001.

[16] J. B. Adams, M. O. Smith, and P. E. Johnson, "Spectral mixture modeling: A new analysis of rock and soil types at the Viking Lander 1 site," *J. Geophys. Res.*, vol. 91, no. B8, pp. 8098–8112, Jul. 1986.

[17] J. J. Settle and N. A. Drake, "Linear mixing and the estimation of ground cover proportions," *Int. J. Remote Sens.*, vol. 14, no. 6, pp. 1159–1177, 1993.

[18] P. M. Mather, *Computer Processing of Remotely-Sensed Images and Introduction*, 3rd ed. West Sussex, U.K.: Wiley, 2004, pp. 203–249.

[19] M. O. Smith, S. L. Ustin, J. B. Adams, and A. R. Gillespie, "Vegetation in deserts: I. A regional measure of abundance from multispectral images," *Remote Sens. Environ.*, vol. 31, pp. 1–26, Jan. 1990.

[20] S. Tompkins, J. F. Mustard, C. M. Pieters, and D. W. Forsyth, "Optimization of endmembers for spectral mixture analysis," *Remote Sens. Environ.*, vol. 59, pp. 472–489, Mar. 1997.

[21] G. I. Metternicht and A. Fermont, "Estimating erosion surface features by linear mixture modeling," *Remote Sens. Environ.*, vol. 64, pp. 254–265, June 1998.

[22] M. A. Theseira, G. Thomas, and C. A. D. Sannier, "An evaluation of spectral mixture modeling applied to a semi-arid environment," *Int. J. Remote Sens.*, vol. 23, no. 4, pp. 687–700, Feb. 2002.

[23] F. Camacho-De Coca, F. J. Garcia-Haro, M. A. Gilabert, and J. Meliá, "Vegetation cover seasonal changes assessment from TM imagery in a semi-arid landscape," *Int. J. Remote Sens.*, vol. 25, no. 17, pp. 3451–3476, Sep. 2004.

[24] P. E. Dennison and D. A. Roberts, "Endmember selection for multiple endmember spectral mixture analysis using endmember average RMSE," *Remote Sens. Environ.*, vol. 87, pp. 123–135, Oct. 2003.

[25] M. A. Theseira, G. Thomas, J. C. Taylor, F. Gemmell, and J. Varjo, "Sensitivity of mixture modeling to end-member selection," *Int. J. Remote Sens.*, vol. 24, no. 7, pp. 1559–1575, Apr. 2003.

[26] T. Schmid, M. Koch, J. Gumuzzio, and P. M. Mather, "A spectral library for a semi-arid wetland and its application to studies of wetland degradation using hyperspectral and multispectral data," *Int. J. Remote Sens.*, vol. 25, no. 13, pp. 2485–2496, Jul. 2004.

[27] M. Koch, "Geological controls of land degradation as detected by remote sensing: A case study in Los Monegros, north-east Spain," *Int. J. Remote Sens.*, vol. 21, no. 3, pp. 457–473, Feb. 2000.

[28] D. A. Roberts, G. T. Batista, J. L. G. Pereira, E. K. Waller, and B. W. Nelson, "Change identification using multitemporal spectral mixture analysis: Applications in Eastern Amazonia," in *Remote Sensing Change Detection Environmental Monitoring Methods and Applications*, R. S. Lunetta and C. D. Elvidge, Eds. Chelsea, MI: Ann Arbor, 1988, pp. 137–161.

[29] J. Gumuzzio, T. Schmid, M. Koch, P. M. Mather, and M. Rodríguez, "Synergetic use of multispectral and hyperspectral data in characterising changes in semiarid wetlands in Spain," in *Proc. 3rd EARSeL Workshop on Imaging Spectroscopy*, Herrsching, Germany, 2003, pp. 206–214.

[30] M. Koch, T. Schmid, J. Gumuzzio, and P. M. Mather, "Evaluation of ASTER and DAIS data for mapping semiarid wetlands in La Mancha, Spain," in *Proc. 3rd EARSeL Workshop on Imaging Spectroscopy*, Herrsching, Germany, 2003, pp. 236–244.

[31] M. Peinado, "Gología y geomorfología," in *Humedales de Ciudad Real*, 1st ed. Talavera de la Reina, Toledo, Spain: Esfagos S. L, 2000, pp. 112–123.
[32] FAO, "World reference base for soil resources," Food Agricult. Org. United Nations, Rome, Italy, Rep. 84, 1998. [Online]. Available: http://www.fao.org/docrep/W8594E/W8594E00.htm.
[33] S. Cirujano and L. Medina, *Plantas Acuáticas de las Lagunas y Humedales de Castilla-La Mancha*. Madrid, Spain: Real Jardín Botánico y Junta de Comunidades de Castilla-La Mancha, 2002, pp. 247–258.
[34] T. Schmid, "Integrated remote sensing approach to detect changes in semi-arid wetland areas in central Spain," Colección Documentos CIEMAT, Madrid, Spain, to be published.
[35] R. Richter, "Atmospheric/topographic correction for wide FOV airborne imagery: Model ATCOR4," DLR, Wessling, Germany, Rep. DLR-IB 552-05/99, 1999.
[36] D. Schläpfer, M. E. Schaepman, and K. I. Itten, "PARGE: Parametric geocoding based on GCP-calibrated auxiliary data," in *Proc. SPIE Conf. Imaging Spectrometry IV*, vol. 3438, San Diego, CA, 1998, pp. 334–344.
[37] B. L. Markham and J. L. Barker, "Landsat MSS and TM post-calibration dynamic ranges, exoatmospheric reflectances and at-satellite temperatures," Earth Observation Satellite Co., Lanham, MD, Landsat Tech. Note 1, Aug. 1986.
[38] D. Williams, Ed., *Landsat-7 Science Data Users Handbook*. Greenbelt, MD: NASA/Goddard Space Flight Center, Mar., 2005. [Online]. Available: http://ltpwww.gsfc.nasa.gov/IAS/handbook/handbook_toc.html.
[39] P. M. Mather, *Computer Processing of Remotely-Sensed Images and Introduction*, 3rd ed. West Sussex, U.K.: Wiley, 2004, pp. 115–118.
[40] P. S. Chavez, Jr., "Image-based atmospheric corrections—Revisited and improved," *Photogramm. Eng. Remote Sens.*, vol. 62, pp. 1025–1036, Sep. 1996.
[41] D. Lu, P. Mausel, E. Brondizio, and E. Moran, "Assessment of atmospheric correction methods for Landsat TM data applicable to Amazon basin LBA research," *Int. J. Remote Sens.*, vol. 23, no. 13, pp. 2651–2671, July 2002.
[42] RSI, *The Environment for Visualizing Images ENVI Version 4.0*. Boulder, CO: Research Systems, Inc., 2003.
[43] A. A. Green, M. Berman, P. Switzer, and M. D. Craig, "A transformation for ordering multispectral data in terms of image quality with implications for noise removal," *IEEE Trans. Geosci. Remote Sensing*, vol. 26, no. 1, pp. 65–74, Jan. 1988.
[44] J. B. Lee, A. S. Woodyatt, and M. Berman, "Enhancement of high spectral resolution remote sensing data by a noise-adjusted principal components transform," *IEEE Trans. Geosci. Remote Sensing*, vol. 28, no. 3, pp. 295–304, May 1990.
[45] J. W. Boardman, F. A. Kruse, and R. O. Green, "Mapping target signatures via partial unmixing of AVIRIS data," in *Summaries of the 5th JPL Airborne Earth Science Workshop*, vol. 1, 1995, JPL Pub. 95–1, pp. 23–26.
[46] J. W. Boardman, "Automated spectral unmixing of AVIRIS data using convex geometry concepts," in *Summaries of the 4th JPL Airborne Geoscience Workshop*, vol. 1, 1993, JPL Pub. 93–26, pp. 11–14.
[47] R. N. Clark, G. A. Swayze, A. Gallagher, N. Gorelick, and F. Kruse, "Mapping with imaging spectrometer data using the complete band shape least-squares algorithm simultaneously fit to multiple spectral features from multiple materials," in *Proc. 3rd Airborne Visible/Infrared Imaging Spectrometer (AVIRIS) Workshop*, 1991, JPL Pub. 91–28, pp. 2–3.
[48] A. J. Elmore, J. F. Mustard, S. J. Manning, and D. B. Lobell, "Quantifying vegetation change in semiarid environments: Precision and accuracy of spectral mixture analysis and the normalized difference vegetation index," *Remote Sens. Environ.*, vol. 73, pp. 87–102, Jul. 2000.
[49] D. Lu, M. Batistella, E. Moran, and P. Mausel, "Application of spectral mixture analysis to Amazonian land-use and land-cover classification," *Int. J. Remote Sens.*, vol. 25, no. 23, pp. 5345–5358, Dec. 2004.
[50] R. G. Bryant, "Validated linear mixture modeling of Landsat TM data for mapping evaporite minerals on a playa surface: Methods and applications," *Int. J. Remote Sens.*, vol. 17, no. 2, pp. 315–330, Jan. 1996.

Thomas Schmid received the M.Sc. degree in geography from the University of Zürich, Zürich, Switzerland, and the Ph.D. degree in science from the Autonomous University of Madrid, Madrid, Spain, in 1993 and 2004, respectively.

He is currently a Researcher at the Department of Environment, Research Centre for Energy, Environment and Technology (CIEMAT), Madrid, since 1994. His main research interests are the implementation of remote sensing and GIS to determine and monitor wetland and soil degradation processes and the effect of heavy metal contamination in semiarid environments.

Magaly Koch received the M.Sc. degree in geology from the University of Cologne, Cologne, Germany, and the Ph.D. degree from Boston University, Boston, MA, in 1986 and 1993, respectively. Her Ph.D. research was on the use of remote sensing in ground water studies.

Her current post is that of Research Associate Professor at the Center for Remote Sensing, Boston University. Her primary research interest is in the application of remote sensing and GIS to the evaluation of water resources and environmental change in arid and semiarid lands.

Jose Gumuzzio received the M.Sc. degree in chemistry (geochemistry) and the Ph.D. degree in chemistry (soil science) from the Autonomous University of Madrid, Madrid, Spain, in 1974 and 1979, respectively.

He is currently a Professor of soil sciences at the Autonomous University of Madrid since 1974, and a Senior Researcher specializing in soil science (UNESCO code: 2511). His main research interest is in the application of remote sensing and GIS to wetland and soil degradation processes and salinity in semiarid environments.